ELSEVIER

Journal of Nuclear Materials 313–316 (2003) 941–946

journal of nuclear materials

www.elsevier.com/locate/jnucmat

Wall conditioning and power balance for spheromak plasmas in SSPX

D.N. Hill *, R.D. Wood, R. Bulmer, H.S. McLean, D. Ryutov, B.W. Stallard, S. Woodruff

Lawrence Livermore National Laboratory, Livermore, CA 94550-0808, USA

Abstract

We report here results from power balance measurements for ohmically heated plasmas in the sustained spheromak physics experiment. The plasma is formed inside a close-fitting tungsten-coated copper shell; wall conditioning by baking, glow discharge cleaning (GDC), Ti gettering, and helium shot conditioning produces clean plasmas ($Z_{\text{eff}} < 2.5$) and reduces impurity radiation to a small fraction of the input energy, except when the molybdenum divertor plate has been overheated. We find that most of the input energy is lost by conduction to the walls (the divertor plate and the inner electrode in the coaxial source region). Recently, carborane was added during GDC to boronize the plasma-facing surfaces, but little benefit was obtained.

Keywords: Spheromak; Boronization; Impurity radiation; Conditioning; Power balance

1. Introduction

The spheromak is a compact toroidal magnetic confinement device in which currents in the plasma self-consistently produce the confining magnetic fields [1]. This eliminates the need for a set of toroidal field and ohmic-heating coils linking the plasma, potentially offering an attractive fusion reactor concept. Spheromak plasmas are typically produced by DC coaxial injection (a Marshall gun) into a close-fitting conducting shell (the flux conserver) required to maintain global stability of the final configuration.

The primary challenge for spheromak development is to show that efficient magnetic field generation is possible while simultaneously maintaining good energy confinement. The reason this is an issue is that, in the spheromak, the toroidal electric field which maintains the toroidal plasma current results from magnetic fluctuations via a plasma dynamo: $E_{\text{dyn}} = \langle \tilde{v} \times \tilde{B} \rangle$ where $\tilde{v}$ and $\tilde{B}$ are the fluctuating fluid velocity and magnetic fields, respectively. In the sustained spheromak physics experiment (SSPX) at Livermore, we are exploring the physics of the magnetic field generation and working to quantify how the magnetic fluctuations affect energy confinement.

It is important to minimize plasma–wall interactions in spheromaks because the efficiency of the magnetic field generation ($\varepsilon = \int B^2 \, dV / P_{\text{in}}$) depends on the plasma resistivity; η, which in turn depends on the electron temperature and Z_{eff} ($\eta \propto Z_{\text{eff}} T_e^{-3/2}$). Furthermore, the current profile in the spheromak is rather flat so that most of the ohmic power is dissipated in the edge, where T_e is low and Z_{eff} can be strongly affected by plasma–wall interactions. In addition, the resistivity has a large impact on MHD behavior and energy confinement because, in steady state, the dynamo electric field must balance the ohmic field, ηj, so that the higher the resistivity, the larger the fluctuations needed to maintain the plasma current [2].

Power balance and energy confinement for present-day, small-scale sustained spheromak plasmas is fundamentally different than for ohmically heated tokamak

* Corresponding author.
E-mail address: hilld@llnl.gov (D.N. Hill).

0022-3115/03/$ - see front matter
PII: S0022-3115(02)01391-0

plasmas because most of the energy is dissipated in generating the confining magnetic field. As much as 75–80% of this dissipation occurs on the open field lines that surround the confined plasma and connect to the driving electrodes in the coaxial source regions, as shown in the SSPX cross-section appearing in Fig. 1. Use of biased electrodes (the coaxial source) to drive the current further complicates power balance because there can be significant losses associated with the electrode sheaths. Since we expect that these losses will become less important in larger, hotter spheromaks [3], it is important that we separate them from the overall power balance, if possible.

In the remainder of this paper we discuss power balance in the SSPX spheromak, which is driven by coaxial helicity injection [4]. Section 2 provides a brief description of the device and plasma conditions, Section 3 covers the power loss measurements, and in Section 4 we discuss the implications of the measurements and present initial results from boronization experiments.

2. Sustained spheromak physics experiment

As in CTX [5] and earlier spheromak experiments [6], we use coaxial helicity injection in SSPX to produce spheromak plasmas inside a 1 m diameter by 0.5 m high 2 cm thick copper flux conserver (plasma volume = 0.4 m^3), as shown in Fig. 1. All the plasma-facing components are coated with a 100 μm thick layer of plasma-sprayed tungsten to minimize sputtering. Use of carbon-based materials has been avoided so that we can successfully remove water with a 165 °C bake. The shape of the flux conserver has been designed to minimize the intersection of open field lines with the surface (like a conformal limiter in a tokamak).

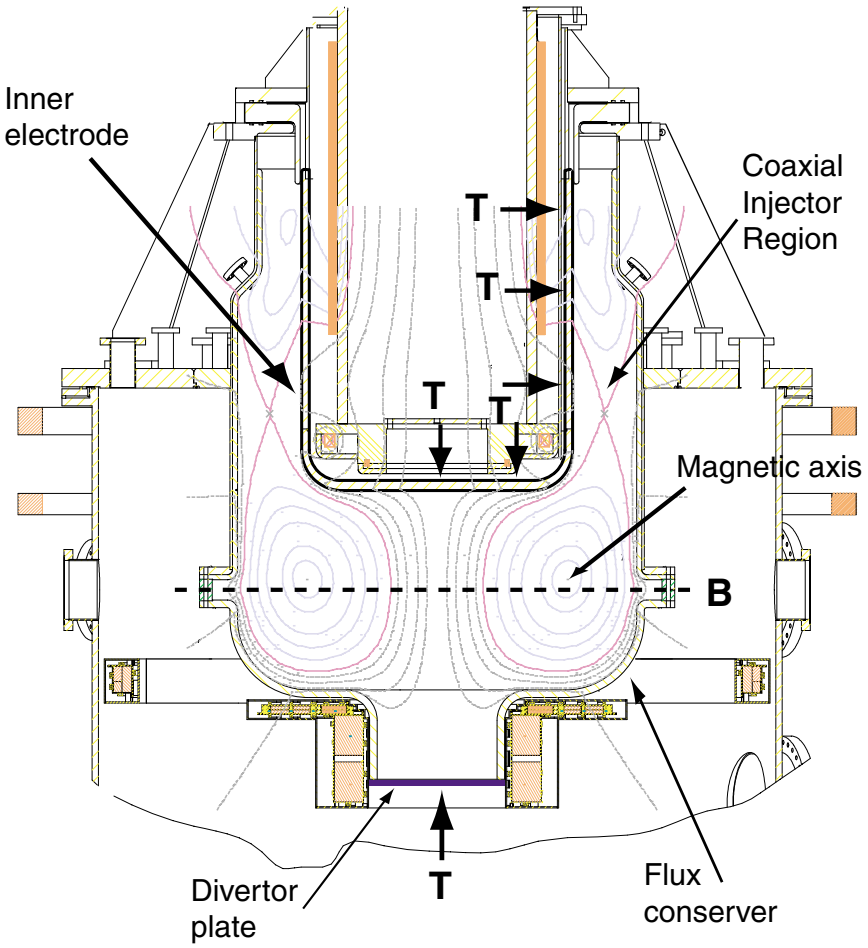

Fig. 1. Cross-section of SSPX showing magnetic flux surfaces for upper divertor case. Diagnostics for power balance are as indicated: B – bolometer view at midplane, T – thermocouples for temperature measurements.

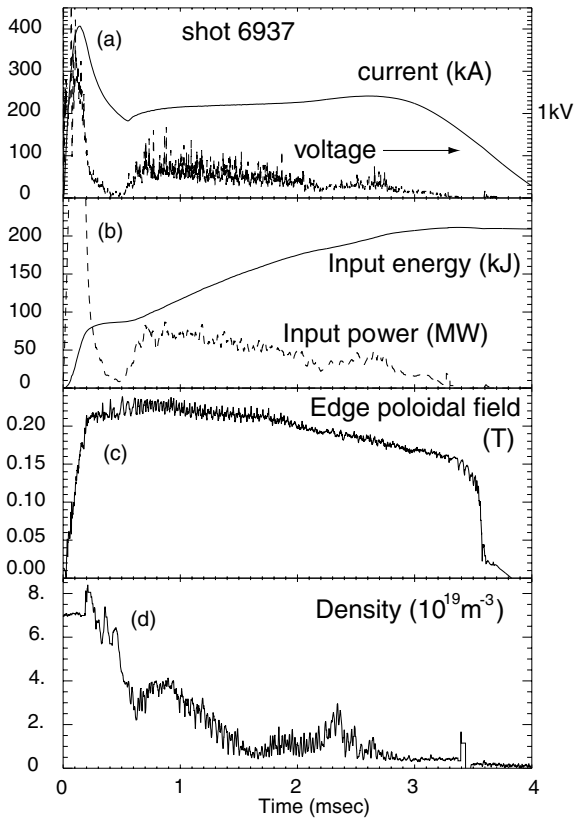

Fig. 2. Time history of typical SSPX discharge: (a) injector current and voltage, (b) input power and energy throughput, (c) spheromak edge poloidal field, (d) line-average density.

Peak *toroidal* plasma current in SSPX has reached 600 kA with sustained pulse lengths of 3.5 ms. Data from a typical discharge appear in Fig. 2. The plasma is formed by first puffing H_2 into the coaxial region where a radial vacuum magnetic field spans the gap. Breakdown follows 250 μs later, when a −6 kV bias is applied to the inner electrode (the cathode): the flux conserver is maintained at ground potential and becomes the outer electrode in the coaxial region. The initial radial current sheet produces a toroidal field in the coaxial gap, which creates a $j \times B_{\mathrm{tor}}$ force that accelerates the plasma with trapped magnetic field down the coaxial region into the flux conserver. The magnetic field inside the flux conserver reaches steady state about 300 μs after the initial breakdown; the magnetic configuration is characterized by nearly force-free field-aligned currents [7], with the fields almost purely poloidal at the edge and completely toroidal on the magnetic axis at the midplane ($R = 0.31$ m in Fig. 1).

Once formed, the spheromak plasma is sustained by maintaining sufficient injector current to keep the field lines pushed out into the flux conserver by local $j \times B$ forces (this minimum is called the sustainment threshold current). The SSPX power supply (a capacitor bank) has relatively high internal impedance, so the spheromak is driven by what amounts to a constant current source. The injector voltage is determined by the total impedance (bulk plasma + sheath) and the circuit current. The plasma impedance contains both a resistive and an inductive component ($R \sim 1$ mΩ and $L \sim 0.5$ μH). The sheath voltage has been estimated to fall in the range 50–100 V, though the exact value and its variation with plasma conditions is not well known [8]. The total input power, calculated as $I_{\mathrm{inj}} V_{\mathrm{inj}}$, steadily drops as the injector voltage falls during the pulse, as shown in Fig. 2. Typically, about 10% of the injected energy ends up in stored magnetic field energy.

The spheromak can operate with a magnetic divertor at bottom of the flux conserver if the initial vacuum magnetic field configuration has field lines that connect the divertor surfaces (functioning as part of the outer electrode) to the inner electrode (cathode). In this case, the open field lines in the scrape-off-layer of the fully formed spheromak plasma will allow electrical current and plasma to flow to the divertor; otherwise, the SOL field lines bypass the lower divertor and connect the inner and outer electrodes up in the coaxial region, as shown in Fig. 1. The SSPX divertor target is presently a simple flat 0.65 cm thick molybdenum plate bolted to the flux conserver to provide a low resistance path for electrical current.

In SSPX, we have used a combination of high temperature baking (165 °C), hydrogen glow discharge cleaning (GDC), helium discharge conditioning, and titanium gettering every 3–4 discharges to produce clean plasmas, defined as having $Z_{\mathrm{eff}} \leqslant 2.5$ as determined from VUV spectroscopy and plasma resistivity [9]. We burn through carbon so that Li-like and Be-like oxygen becomes the main source of impurity radiation. Peak plasma temperatures over 250 eV have been measured with our Thomson scattering system. The best performance is obtained when the plasma is driven at current levels which are close to the sustainment threshold (defined above) which minimizes magnetic fluctuations [10].

Recently, we introduced carborane into SSPX during helium GDC in an attempt to boronize the plasma-facing surfaces [11–13]. Carborane ($C_2B_{10}H_{12}$) is a solid at room temperature, but its vapor pressure begins rising sharply near 70 °C. Experiments have shown that boronization can be accomplished by introducing the carborane vapor into a helium glow discharge plasma. In our case, we introduced the carborane during baking when the vessel interior was at 165 °C. The GDC pressure was 80 mTorr (to reach up into the coaxial injector), with 90% helium and 10% carborane (regulated via the carborane temperature). We maintained the glow for 8 h. Analysis of coupons placed at the flux conserver wall showed that the surface had the lowest boron

fraction: B:C = 1:1.9 at the surface of the 180 nm film compared to B:C = 2.3:1 at base.

3. Power balance measurements

We measure the energy loss from the spheromak in three locations: (1) the inner electrode (discharge cathode), (2) the divertor plate (anode), and (3) the plasma midplane. The measurements at the electrodes are sensitive to both plasma and radiative/charge-exchange heating, while the midplane measurement is via a bolometer that is shielded from plasma contact and so is sensitive only to radiation and charge exchange losses.

We measure the spatial distribution of energy deposited on the inner electrode using a set of five thermistors positioned as shown in Fig. 1. The inner electrode is made of copper 1.9 cm on the sides and 2.54 cm thick on the bottom; the thermistors were epoxied to the back side. Calculated front-to-back thermal diffusion times are less than 1 s, whereas the time for the heat to redistribute across the surface is observed to be several minutes. Therefore, each measurement is assumed to represent local, toroidally symmetric electrode heating; summing the contributions from each measurement zone provides the total energy deposition on the electrode.

Fig. 3 shows inner electrode thermal data from 41 sustained discharges in SSPX, plotted against the integrated input energy. While there is a fair amount of scatter, on average we observe that 22% of the injected energy ends up on the inner electrode. Typically, 80% or more of the electrode heating occurred on the lower half of the electrode, distributed fairly evenly between the three thermistors used to measure it. Most of this heating must result from direct ion bombardment because the fraction of input energy is too large to result from radiative loads, as the bottom of the electrode represents only 12% of the flux conserver surface area and the radiation fraction is usually well below 50% of the energy input.

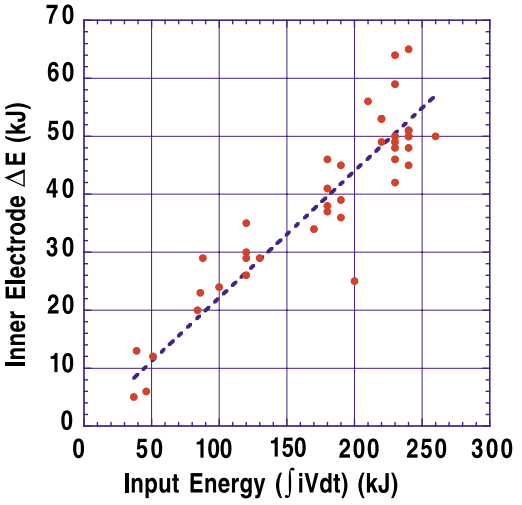

Fig. 3. Inner electrode heating as a function of input energy for sustained discharges. Dashed line is a linear fit to the data: $E_{\text{electrode}} = 0.22E_{\text{input}}$.

Normally, we expect most of the injector current to return to the outer electrode within the coaxial source region because the magnetic fields nominally should be tangential to the flux conserver surface everywhere else. However, some vacuum magnetic field configurations obtained using a additional set of programmable bias coils (designated BCM and BCS configurations to differentiate between field line curvature near the bottom of the inner electrode) have field lines connecting the inner electrode to the bottom of the flux conserver so current flow between these two surfaces is possible. We can detect the current returning to the lower half of the flux conserver using Rogowski coils mounted at the midplane diagnostic slot.

We installed a 6 mm thick molybdenum divertor plate at the very bottom of the flux conserver to intercept the plasma when operated in these configurations. The temperature of the plate was monitored by a single thermocouple at the center; the temperature reached 90% of its final value within 1 s, as expected from the thermal properties of molybdenum. Visual inspection of the plate showed fairly uniform surface damage (melting) confined to the region intercepted by the magnetic field lines (22 cm in diameter) which reach the plate; this suggests that the heating was fairly uniform. Thus, in calculating the energy deposition, we assumed uniform deposition.

Significant heating of the divertor plate was observed only when a large fraction of the vacuum magnetic flux intercepted the divertor plate (i.e., in the BCS or BCM configurations), as shown in Fig. 4. In these cases, as much as 80% of the input energy was deposited on the plate when operating at the highest injector voltages. The fraction dropped to 50% at lower voltages. At high voltage, the energy deposition was estimated to be sufficient to produce surface melting of the divertor targets, which was confirmed by later visual inspection. Discharges in with the highest deposition where characterized by high radiation fractions and rapid rise in plasma density.

Radiative and charge exchange losses were measured using a bolometer at the plasma midplane. The bolometer measured the total integrated loss from a thin (2 cm thick) horizontal slice using a small 1 mm diameter thermistor situated behind a limiting horizontal slit. The unit was calibrated in situ using electrical heat pulses and off-line using a thermal bath. With the present ge-

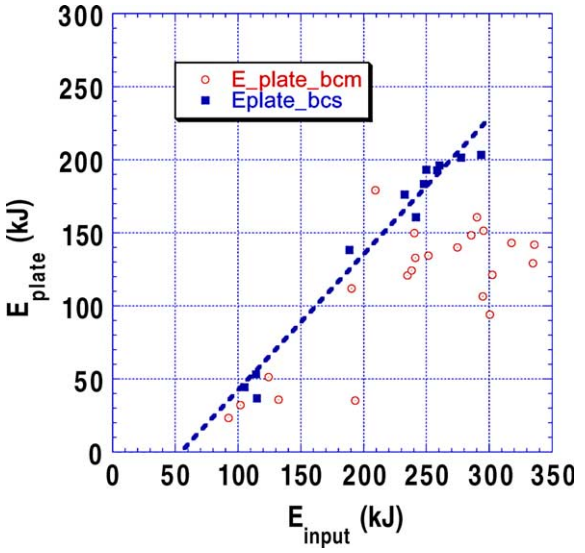

Fig. 4. Divertor plate energy as a function of input energy for the BCS and BCM magnetic configurations (see text). Dashed line is linear fit to the BCS data only.

ometry, the bolometer was not sensitive to radiation loss from the divertor or injector regions and so measured losses primarily from the spheromak plasma inside the separatrix.

In clean plasmas with $Z_{\text{eff}} < 2.5$, which showed only emission from Li-like states of oxygen, the radiation losses were typically about 15% of the input energy for a wide range values. We did not find a correlation between core plasma density and time average radiation losses within our power balance database of over 100 discharges, but this may reflect the fact that the density measurement is time-resolved and the radiation loss is time-integrated. Without gettering and conditioning with helium plasmas, carbon radiation became significant and the radiation fraction climbed to 50% or more. When melting of the divertor plate was inferred from the heat flux measurements, a sharp rise in radiation loss was observed, suggesting that significant contamination from metallic impurities (not easily identified by a VUV spectrometer) occurred.

4. Discussion and conclusions

Power balance for a large number (~100) of SSPX sustained spheromak plasmas with similar operating conditions and $Z_{\text{eff}} \leqslant 2.5$ is summarized in Table 1 below. The averages were computed separately since we did not make all three measurements simultaneously on all the discharges (we usually measured two out of the three components of the power balance on any given discharge). Three quarters of the input energy is deposited on the current carrying electrodes (inner electrode in the coaxial region and the divertor plate). The inner electrode heating is consistent with the measured discharge current and the sheath voltage inferred from helicity balance and circuit analysis (~100 V). This is somewhat lower than the cathode sheaths reported for linear discharges [14], which are typically near the Paschen minimum voltage (~280 V for H_2) required to initiate the discharge. Most of the cathode heating should be due to ion impact, since the electrode is negatively biased. Heating of the inner electrode due to line radiation and charge exchange is estimated to be less than 30% of this.

Table 1
Power balance for clean SSPX discharges

Region/surface	Energy relative to $\int IV\,dt$ (%)
Inner electrode (cathode)	22
Midplane radiation and CX	15
Divertor plate (anode)	55
Total measured	92

The large heat flux at the divertor plate (discharge anode) results from two effects: (1) the applied bias allows a higher fraction of the electrons to hit the target, and (2) the electron fluid arrives at the plate with finite flow velocity and higher temperature due to ohmic heating in the collisional edge plasma. The electrons do not acquire significant parallel kinetic energy from the applied electric field because their collisional mean free path is 10% or less of the connection length. In these conditions, the spatial distribution of the heat flux is governed by the current density rather than perpendicular transport.

We introduced boron into the spheromak to reduce the observed oxygen radiation, with the hope that this would lower the radiative losses and yield improved confinement and higher temperature plasmas. After we boronized via vaporization of carborane into a helium glow discharge, we found that density control became difficult (presumably due to hydrogen codeposition during GDC with subsequent release by ion impact), producing very high density plasmas ($n_e \sim 4 \times 10^{20}$ m^{-3} compared to the usual 5×10^{19} m^{-3}). The high density lowered the plasma temperature significantly (to about 50 eV). Further, VUV spectroscopy showed increased carbon radiation (larger than oxygen, which did not change). We speculate that the high measured carbon fraction in the coating increased hydrocarbon production by plasma bombardment of the flux conserver surfaces. The fact that the oxygen lines did not change compared to our previous conditions may reflect the fact that titanium gettering is an equally efficient trap for O_2. We are now looking into other methods for depositing boron on the first walls of SSPX.

The high heat flux challenges high power or long-pulse operation in SSPX when the vacuum magnetic field is pulled onto the divertor plate rather than allowed to intercept a larger area on the walls of the flux conserver. We have begun conceptual design of a new divertor target to spread out the heat flux, which can be as high as 500 MW/m^2 parallel to the field lines in SSPX. Radiative divertor solutions will probably not be useful for our present short pulse-length discharges and will unnecessarily complicate confinement experiments.

Acknowledgements

This work was carried out by LLNL under the auspices of the US Department of Energy Contract Nos. W-7405-ENG-48.

References

[1] T.R. Jarboe, Plasma Phys. Control. Fusion 36 (1994) 945.
[2] T.K. Fowler, Fusion Technol. 29 (1996) 206.
[3] R.L. Hagenson, R.A. Krakowski, Fusion Technol. 8 (1985) 1606.
[4] J.B. Taylor, M.F. Turner, Nucl. Fusion 29 (1989) 219.
[5] C.W. Barnes, T.R. Jarboe, I. Henins, et al., Nucl. Fusion 24 (1984) 267.
[6] W.C. Turner, E.H.A. Granneman, C.W. Hartman, et al., J. Appl. Phys. 52 (1981) 175.
[7] J.B. Taylor, Rev. Mod. Phys. 58 (1986) 741.
[8] B.W. Stallard, D.N. Hill, C. Holcomb, 28th EPS Conference on Controlled Fusion and Plasma Physics, Madeira, Portugal, 2001.
[9] R.D. Wood, D.N. Hill, E.B. Hooper, et al., J. Nucl. Mater. 290–293 (2001) 513.
[10] H.S. McLean, S. Woodruff, E.B. Hooper, et al., Phys. Rev. Lett. 88 (2002) 125004.
[11] O.I. Buzhinsky, Y.M. Semenets, Fusion Technol. 32 (1997) 1.
[12] V.M. Sharapov, S.V. Mirnov, S.A. Grashin, et al., J. Nucl. Mater. 220–222 (1995) 730.
[13] O.I. Buzhinsky, E.A. Azizov, A.M. Belov, et al., J. Nucl. Mater. 191–194 (1992) 1413.
[14] L.B. Loeb, Fundamental Processes of Electrical Discharge in Gases, Wiley, New York, 1939.